scientific reports

Check for updates

OPEN

A comprehensive analysis of advanced solar panel productivity and efficiency through numerical models and emotional neural networks

Ali Basem[1], Serikzhan Opakhai[2], Zakaria Mohamed Salem Elbarbary[3]✉, Farruh Atamurotov[4,5,6] & Natei Ermias Benti[7]✉

This study presents an in-depth analysis and evaluation of the performance of a standard 200 W solar cell, focusing on the energy and exergy aspects. A significant research gap exists in the comprehensive integration of numerical models with advanced machine-learning approaches, specifically emotional artificial neural networks (EANN), to simulate and optimize the electrical characteristics and efficiency of solar panels. To address this gap, a numerical model alongside a novel EANN was employed to simulate the system's electrical characteristics, including open-circuit voltage, short-circuit current, system resistances, maximum power point characteristics, and characteristic curves. Mathematical equations for calculating efficiency levels under varying operational conditions were developed. The system's operational and electrical parameters, alongside environmental conditions such as solar radiation, wind speed, and ambient temperature, were empirically observed and documented over a day. A comparative analysis was conducted to validate the model by comparing its results with manufacturer data and experimental observations. During the trial from 7:00 to 17:00, energy efficiency varied from 10.34 to 14.00%, averaging 13.6%, while exergy efficiency ranged from 13.57 to 16.41%, with an average of 15.70%. The results from the EANN model indicate that the proposed method for forecasting energy, exergy, and power is feasible, offering a significant reduction in computational expense compared to traditional numerical models. The integration of numerical modeling with EANN enhances simulation accuracy and the developed equations enable real-time efficiency calculations. Empirical validation under varying environmental conditions improves predictive capabilities for solar panel performance. Additionally, operational efficiency assessments aid in better design and deployment of solar energy systems, and computational costs for large-scale solar energy simulations are reduced.

Keywords Solar cell, Comparative analysis, Environmental conditions, Energy and exergy efficiency, Machine-learning

The adoption of alternative energy sources like solar energy, ocean waves, geothermal energy, etc. will revolutionize the contemporary world as a result of the constraints posed by finite energy resources such as fossil fuels[1–4]. The growing demand for renewable energy sources has led to significant advancements in solar technology, particularly in the efficiency and productivity of solar panels[5–7]. The uninterrupted and consistent provision

[1]Air Conditioning Engineering Department, Faculty of Engineering, Warith Al-Anbiyaa University, Karbala, Iraq. [2]Faculty of Physics and Technical Sciences, L.N. Gumilyov Eurasian National University, 010000 Astana, Kazakhstan. [3]Electrical Engineering Department, College of Engineering, King Khalid University, Abha, Saudi Arabia. [4]New Uzbekistan University, Movarounnahr street 1, 100000 Tashkent, Uzbekistan. [5]University of Public Safety of the Republic of Uzbekistan, 100109 Tashkent, Tashkent Region, Uzbekistan. [6]University of Tashkent for Applied Sciences, Str. Gavhar 1, 100149 Tashkent, Uzbekistan. [7]Computational Data Science Program, College of Computational and Natural Science, Addis Ababa University, P.O. Box 1176, Addis Ababa, Ethiopia. ✉email: albrbry@kku.edu.sa; natei.ermias@aau.edu.et

of energy has always been a fundamental requirement for human beings. Fossil fuel sources have long been the primary energy provider[8–10]. Nevertheless, obstacles of notable concern include environmental pollution and constraints on the availability of various fuel sources[11–13]. Novadays, various nations are actively seeking to create and utilize renewable energy sources as sustainable and environmentally friendly alternatives[14]. This is done with the aim of decreasing dependence on fossil fuels and safeguarding the natural environment[15–17]. Solar energy is a crucial source of power that may be harnessed and turned into useful electrical energy through the use of solar panels[18–20]. The assessment and examination of these panels in relation to energy and exergy is the fundamental initial stage in the advancement of this technology, offering an appropriate standard for appraising the efficiency of solar panels[21–23]. The analysis of energy is grounded in the fundamental principles of the first law of thermodynamics, whereas the analysis of exergy is rooted in the underlying principles of the second law of thermodynamics. Exergy analysis is commonly employed as a superior method for evaluating equipment performance. Unlike energy analysis, which solely considers the quantity of energy input and output, exergy analysis plays a more significant role in assessing the efficiency of physical and chemical processes. Exergy analysis focuses on the capacity to perform work and examines energy in terms of its exergy and energy that is unable to be converted into work (irreversibility)[24–26].

Recently, solar cells have become a viable and environmentally friendly energy source, providing both electricity and heat[27,28]. Significantly, technological progress has driven the advancement of photovoltaic-thermal systems, which have the capability to simultaneously generate electricity and heat. These cells have been thoroughly investigated in numerous research, utilizing different methods to measure their effectiveness, with a particular emphasis on their electrical and thermal properties[29–32]. This is especially important when considering cells used for thermal purposes. The operational efficiency of these systems depends on various crucial elements, including rated power, distinct internal resistances within the cell, operating voltage and current, short-circuit current, and open-circuit voltage. Factors like the intensity of radiation, the speed of the wind, the surrounding temperature, the properties of the cell surface, and the coefficients of heat transfer are crucial in properly constructing these systems. Developing a comprehensive model that considers all the necessary components is essential for precisely assessing and examining the effectiveness of a solar system, guaranteeing a precise understanding of its performance. Considerable research has explored the field of energy and exergy analysis of solar panels owing to their significant significance[33–35].

In recent years, extensive research has been conducted to enhance the efficiency and reliability of solar panel systems. Allouhi et al.[36] stated that heat pipes integrated with flat plate collectors as heat extraction devices are a promising alternative to conventional systems. This configuration may potentially overcome specific limitations identified in flat plate collectors. A comprehensive evaluation was carried out to analyze the transient performance of a forced circulation solar water heating system that utilizes a heat pipe flat plate collector. The assessment covered evaluations conducted on an hourly and daily basis, which included the measurement of solar fraction, thermal collector efficiency, and exergetic efficiency. The inquiry findings indicate that the solar water heating system can maintain a thermal efficiency of up to 33% and an energy efficiency of 4%. It also maintains a daily solar fraction of over 58%, even in the coldest month of the year. Mohammed et al.[37] studied a 200 MW steam cycle power plant for energy and exergy. Find out how feed water heaters (FWH) numbers effect cycle performance. Natural gas combustion, SCPP enthalpy, energy, and entropy changes were in our computer model. Analyzing system irreversibility and power system upgrade prospects requires determining component system degradation exergy and efficiency. The analysis indicated 37.52% energy and 41.7% exergy efficiency for SCPP. SCPP exhausts 48% of gas exergy in the combustion chamber (boiler). Makhdomi et al.[38] addressed the issue of design, economic evaluation of the use of energy storage systems (ESSs) and solar tracking and focused on the optimal size of hybrid energy systems that studied different types of tracking systems. Two hybrid energy systems, namely Diesel/PV/pumped hydraulic storage (PHS) and diesel/PV/fuel cell (FC), were created with distinct tracking methods to achieve the most efficient design. The objective of this design was to reduce two main factors: the total net present cost (TNPC) and the reliability index, which is measured by the power supply loss probability (LPSP), using a multi-objective approach. Due to the complex nature of this optimization issue, a very efficient multi-objective strategy was utilized for resolution. The simulation results showed that using PHS as the energy storage system significantly reduced the TNPC of the hybrid system compared to using FC. Furthermore, the cost-effectiveness of implementing solar trackers in Diesel/PV/PHS systems was determined to be inferior in comparison to utilizing stationary PV panels. Hatami et al.[39] introduced a dynamic model that incorporates the computation of solar energy received on the tiled surface of the collector, temperature variations along the length of the collection, kinetics of moisture reduction, and temperature fluctuations of the desiccant. The researchers conducted thermal analysis by employing both energy and exergy analysis techniques. The findings demonstrated a strong correlation between the model and the experimental data.

Ghadikolaei[40] and Sharaf et al.[41] declared advanced cooling techniques to address the thermal management of PV cells, finding that effective cooling can significantly enhance performance and longevity. Ali Sadat et al.[42] and Jaszczur et al.[43] focused on the detrimental effects of dust accumulation on solar panels, emphasizing the need for regular maintenance and innovative anti-dust solutions to maintain high efficiency. AlShafeey and Csáki[44] applied neural network models to predict PV energy output, achieving high accuracy and demonstrating the potential of machine learning in optimizing solar power systems. Nwokolo et al.[45] combined numerical simulations with machine learning to develop a hybrid model for solar power forecasting, significantly improving prediction accuracy and aiding in better energy management.

Despite these advancements, challenges remain in optimizing solar panel performance under varying environmental conditions. To fill these gaps by presenting an in-depth analysis of solar panel efficiency using a numerical model integrated with an emotional artificial neural network (EANN) could be efficient. The EANN approach introduces a novel way to model and predict solar panel performance by incorporating emotional factors into the neural network, potentially leading to more accurate and responsive energy output predictions.

Consequently, there has been a significant emphasis in recent years on conducting experimental studies related to both photovoltaic cells and photovoltaic-thermal systems. These studies investigate the effects of different working fluids, cell types, cooling processes, presence of solar trackers, and cell shapes on the efficiency of solar systems. This study focuses on evaluating the efficiency of a 200-W solar panel through comprehensive energy and exergy assessments. Input data of this assessment are meteorological variables such as radiation intensity, wind speed, and temperature. These curves have been confirmed by comparing them with the curves provided by the manufacturer. This study introduced a comprehensive machine-learning model based on an EANN, accompanied by the development of a numerical and experimental model, to evaluate the effectiveness of different types of solar cells. The proposed model provides the capacity to replicate electrical performance and comprehensively assess system efficiency. Furthermore, a practical model has been utilized for the aim of validation, enhancing the study by incorporating experimental analysis. This study comprehensively examines various photovoltaic cells, integrating theoretical modeling for performance assessment, and experimental verification. Consequently, it establishes a valuable correlation between theoretical projections and practical outcomes. This study not only advances the theoretical understanding of PV efficiency but also offers practical implications for the design and management of more reliable and efficient solar energy systems.

Energy and exergy analysis

In order to assess the efficiency of solar panels, the first step is obtaining their electrical characteristic curves. These charts depict the correlation between the voltage, current, and power output of the system under varying radiation and temperature conditions. The data derived from these electrical characteristic curves provides the basis for undertaking thorough energy and exergy analyses. In the next step, a comprehensive analysis of the solar panel's energy and exergy is conducted, utilizing precise equations and connections that regulate energy efficiency and exergy principles. This section describes the modeling process and explains the governing equations utilized in this assessment.

The fundamental principle of modeling in this study is represented by Eq. (1), which articulates the correlation between current and voltage in a circuit with constant radiation intensity and temperature.

$$I = I_L - I_D - I_{sh} = I_L - I_o\left[\exp\left(\frac{V - IR_s}{a}\right) - 1\right] - \frac{V + IR_s}{R_{sh}} \tag{1}$$

The variable $I_o(A)$ represents the reverse saturation current or dark current of the diode, whereas $a(V)$ represents the adjusted ideality factor. The diode reverse saturation current, also known as dark current, is the least current required to create an n-p pair in the semiconductor. The value of the coefficient a is determined by the desirability coefficient and other physical parameters. The value of n is 1 for an ideal diode and ranges between 1 and 2 for a non-ideal diode.

Equation (1) necessitates the values of five components, namely I_L, I_D, I_{sh}, R_s, and a, to determine the current in relation to voltage under various operating situations. By plugging in the given values into Eq. (1), and using the temperature coefficient of short circuit current and open circuit voltage, Eqs. (2–6) are derived. These equations allow for the calculation of the values of the five components specified. Subsequently, by employing relations 8–12, the correlation between the values of these components under various operating conditions and their values under reference conditions is created. Ultimately, by utilizing Eq. (1), the current values are derived based on the voltage.

Equation (2) pertains to the short circuit conditions, where the voltage is zero and the current is denoted as $I_{\mathrm{sc,ref}}$ By substituting these values into the Eq. (1) [46].

$$I_{sc,ref} = I_{L,\,\mathrm{ref}} - I_{o,ref}\left[\exp\left(\frac{I_{sc,ref}R_{s,ref}}{a_{\mathrm{ref}}}\right) - 1\right] - \frac{I_{\mathrm{sc,ref}}R_{\mathrm{s,ref}}}{R_{\mathrm{sh,ref}}} \tag{2}$$

Equation (3) pertains to the open circuit situations, where the current is zero and the voltage is constant. Equation (4) relates to the point of greatest power, with its current and voltage values denoted as a and b, respectively.

$$I_{L,\,\mathrm{ref}} = I_{\mathrm{o,ref}}\left[\exp\left(\frac{V_{\mathrm{oc,ref}}}{a_{\mathrm{ref}}}\right) - 1\right] + \frac{V_{\mathrm{oc,ref}}}{R_{\mathrm{sh,ref}}} \tag{3}$$

$$I_{\mathrm{mp.ref}} = I_{\mathrm{L.ref}} - I_{\mathrm{o,ref}}\left[\exp\left(\frac{V_{\mathrm{mp,ref}} + I_{\mathrm{mp,ref}}R_{\mathrm{s,ref}}}{a_{\mathrm{ref}}}\right) - 1\right] - \frac{V_{\mathrm{mp,ref}} + I_{\mathrm{mp,ref}}R_{\mathrm{s,ref}}}{R_{\mathrm{sh,ref}}} \tag{4}$$

The rate of change of electric power with respect to the voltage at the point of maximum power is zero. From this, Eq. (5) is derived. Equation (6) ensures that the model can accurately forecast the temperature coefficient of the open circuit voltage [47].

$$\frac{I_{\mathrm{mp.ref}}}{V_{\mathrm{mp,ref}}} = \frac{\frac{I_{\mathrm{o,ref}}R_{\mathrm{s,ref}}}{a_{\mathrm{ref}}}\exp\left(\frac{V_{\mathrm{mp,ref}} + I_{\mathrm{mp,ref}}R_{\mathrm{s,ref}}}{a_{\mathrm{ref}}}\right) + \frac{1}{R_{\mathrm{sh,ref}}}}{1 + \frac{I_{\mathrm{o,ref}}}{a_{\mathrm{ref}}}\exp\left(\frac{V_{\mathrm{mp,ref}} + I_{\mathrm{mp,ref}}R_{\mathrm{s,ref}}}{a_{\mathrm{ref}}}\right) + \frac{R_{\mathrm{s,ref}}}{R_{\mathrm{sh,ref}}}} \tag{5}$$

$$\frac{\partial V_{oc}}{\partial T} = \mu_{V,oc} \approx \frac{V_{oc}(T_c) - V_{oc}\left(T_{c,ref}\right)}{T_c - T_{c,\,\mathrm{ref}}} \tag{6}$$

The variable $\mu_{V,oc}(\frac{V}{K})$ represents the temperature coefficient of the open circuit voltage, whereas the variable $T_c(K)$ represents the temperature of the cell. As previously stated, coefficient a is contingent upon both the coefficient of desirability and physical characteristics. Equation (7) represents the correlation between variable a and variable n.

$$a \equiv \frac{nkT_cN_s}{q} \tag{7}$$

where k represent the Boltzmann constant, q represent the electrical charge, and N_s represent the number of cells in series. Equation (7) states that the coefficient a varies in a linear manner with temperature. Hence, the value of it under operational circumstances will be derived from Eq. (8).

$$\frac{a}{a_{ref}} = \frac{T_c}{T_{c,ref}} \tag{8}$$

The relationship between I_L and instantaneous radiation exhibits a nearly linear pattern. Indeed, certain radiometers regard the short circuit current of the cell as an indicator of the quantity of radiation. This issue is apparent in Eq. (9).

$$I_L = \frac{S}{S_{ref}}\left[I_{L,ref} + \mu_{l,sc}\left(T_c - T_{c,ref}\right)\right] \tag{9}$$

The variables in question are as follows: S represents the radiation intensity, S_{ref} represents the effective absorption ratio of the panel, and k is the temperature coefficient of the short circuit current. In addition, the value of $\mu_{l,sc}$ in operational conditions will be determined based on Eq. (10) and the corresponding conditions.

$$\frac{I_o}{I_{\text{o.ref}}} = \left(\frac{T_c}{T_{c,ref}}\right)^3 \exp\left(\frac{E_g}{kT}\bigg|_{T_{c,ref}} - \frac{E_g}{kT}\bigg|_{T_e}\right), \frac{E_g}{E_{\text{g.ref}}} = 1 - C\left(T_c - T_{c,ref}\right) \tag{10}$$

The energy gap of the cell material, denoted as E_g, is 1.12 eV and C = 0.00026 for silicon. The shunt resistance, denoted as R_{sh}, is independent of temperature and solely reliant on the intensity of the radiation. As stated in Eq. (11), it exhibits an inverse correlation with the radiation intensity.

$$\frac{R_{sh}}{R_{\text{sh,ref}}} = \frac{S_{\text{ref}}}{S} \tag{11}$$

Furthermore, it can be reasonably inferred that the variations in series resistance due to fluctuations in temperature and radiation intensity are negligible. Therefore, we can conclude:

$$R_s = R_{s,ref} \tag{12}$$

By utilizing Eqs. (8–12), the connection between the reference values and the operational values of all parameters is made, so completing the electrical modeling using the provided method. The modeling will generate power and current diagrams for the solar panel, specifically in relation to voltage, under varying temperatures and radiation intensities. Specifically, the current and voltage corresponding to the maximum power point are determined by solving Eq. (1) and using Eq. (13).

$$I_{mp} = I_L - I_o\left[\exp\left(\frac{V_{mp} - I_{mp}R_s}{a}\right) - 1\right] - \frac{V_{mp} + I_{mp}R_s}{R_{sh}}, \frac{I_{mp}}{V_{mp}} = \frac{\frac{I_o}{a}\exp\left(\frac{V_{mp}+I_{mp}R_s}{a}\right) + \frac{1}{R_{sh}}}{1 + \frac{R_s}{R_{sh}} + \frac{I_oR_s}{a}\exp\left(\frac{V_{mp}+I_{mp}R_s}{a}\right)} \tag{13}$$

Once the system's features are defined and its coefficients are established, Eq. (13) provide the essential inputs for conducting energy and exergy analysis.

The energy efficiency of a solar panel is determined by calculating the ratio of the electrical power produced by the panel to the amount of energy it receives from sunshine. Evidently, the value is contingent upon the magnitude of radiation and the prevailing temperature. Additionally, when determining the energy efficiency, it is presumed that the panel operates under optimal conditions, extracting the greatest electrical power possible given the temperature and operational radiation[48,49]. Additionally, it is presumed that the surface temperature is uniform throughout all the panels, a plausible assumption. Equation (14) is used to compute the value of η_{en} based on the given panel energy efficiency assumptions.

$$\eta_{en} = \frac{V_{mp} \times I_{mp}}{A \times S} \tag{14}$$

where $A(\text{m}^2)$ represent the area of the panel. The values of V_{mp} and I_{mp} are determined using mathematical modeling. The radiation intensity in this research is determined by experimental means.

The exergy efficiency of solar panels can be defined as the ratio of the total output exergy to the total exergy of solar radiation (input exergy), as represented by the Eq. (15).

$$\eta_{\text{ex}} = \frac{Ex_{\text{out}}}{Ex_{\text{in}}} \tag{15}$$

where Ex_{out} represents the output exergy and Ex_{in} represents the input exergy. Only the exergy of solar radiation is considered in the input exergy, and it is computed using Eq. (16).

$$Ex_{\text{in}} = AS\left[1 - \frac{4}{3}\left(\frac{T_a}{T_{\text{sun}}}\right) + \frac{1}{3}\left(\frac{T_a}{T_{\text{sun}}}\right)^4\right] \tag{16}$$

where T_a represents the temperature of the environment and T_{sun} represents the temperature of the sun. Output exergy comprises thermal exergy and electrical exergy. The calculation of thermal exergy is performed using Eq. (17).

$$Ex_{th} = (h_{\text{conv}} + h_{\text{rad}})A(T_c - T_a)\left[1 - \frac{T_a}{T_c}\right] \tag{17}$$

where h_{conv} represents the coefficient for heat transfer due to displacement, and h_{rad} represents the coefficient for heat transfer due to radiation. The heat transfer coefficients for convection and radiation are determined using Eq. (18) [50,51].

$$h_{\text{conv}} = 2.8 + 3v_w, h_{\text{rad}} = \varepsilon\sigma\left(T_{sky} + T_c\right)\left(T_{sky}.^2 + T_c.^2\right) \tag{18}$$

where v_w represent the wind speed, ε represent the emissivity of the panel, σ represent the Stefan-Boltzmann constant, and T_{sky} represent the effective temperature of the sky. The effective temperature of the sky is estimated to be six degrees lower than the ambient temperature, using an appropriate approximation.

Equation (19) shows how to approximate the cell surface temperature using the nominal working temperature of the cell. In this equation, the subscript T_{NOCT} represents the parameter values associated with the nominal working temperature of the cell, while τα represents the effective transmission-absorption coefficient.

$$\begin{aligned} &\frac{T_c - T_a}{T_{NOCT} - T_{a,NOCT}} = \frac{S}{S_{NOCT}} && \text{Method 1} \\ &\frac{T_c - T_a}{T_{NOCT} - T_{a,NOCT}} = \frac{S}{S_{NOCT}} \frac{9.5}{(5.7 + 3.8v_w)}\left[1 - \frac{\eta_{en}}{\tau\alpha}\right] && \text{Method 2} \end{aligned} \tag{19}$$

The electrical exergy and the exergy destruction can be calculated using Eqs. (20) and (21), respectively.

$$Ex_{el} = V_{mp} \times I_{mp} \tag{20}$$

$$Ex_{\text{loss}} = Ex_{in} - Ex_{el} - Ex_{th} \tag{21}$$

The study utilized a solar panel model, the F200P-24. An analysis is conducted on the energy and exergy aspects of the panel's performance throughout the time period from 7 a.m. to 5 p.m. The power plant inverter operates dynamically by continuously determining the operating point that maximizes power generation efficiency. As a result, the output voltage and current of the panel will correspond to the maximum power point. At the location of peak power, measurements are taken for ambient temperature, radiation intensity, wind speed, voltage, and current. Tables 1 and 2 present, respectively, the study's input parameters and the properties of the solar panel under evaluation, both as provided by the manufacturer under reference conditions.

Proposed model

Artificial neural networks (ANN), inspired by the intricate workings of the human brain, are computational models that mimic its structure. These networks comprise interconnected computational units termed neurons or nodes, linked by weighted connections[52]. Each neuron integrates specific inputs from preceding neurons, incorporating designated weights, to generate an output[53]. Within materials and methods research, neural networks serve as computational aids across diverse applications, capitalizing on their capacity to discern and generalize patterns from data via iterative training. Throughout training, network weights undergo adjustments to enhance the model's efficacy in tasks such as classification, regression, and pattern recognition. This adaptive

Input parameters	Value
Working temperature	48
Radiation intensity	850
Ambient temperature	30
Panel emission coefficient	0.85
Effective transmission-absorption coefficient	0.85
Solar temperature	5940

Table 1. Input parameters detail.

Input parameters	Value
Maximum power	200
Open circuit voltage	44.9
Short circuit current	5.7
Maximum power point voltage	36.0
Resistance	5.3
Series resistance	0.9
Temperature coefficient of short circuit current	0.0005
Dimensions (mm)	1580*808*45

Table 2. Solar panel specifications.

nature enables neural networks to furnish predictions grounded in input data, rendering them indispensable tools across scientific and engineering domains[54,55].

EANN models epitomize a refined advancement from ANN models. They incorporate a synthetic sensing mechanism capable of releasing hormones to modulate neuron or node activity. The weight of these hormones varies based on node input and output values. Each node within the EANN generates dynamic hormones, H_a, H_b, and H_c, facilitating continual information exchange between input and output components through a dynamic hormone generator. During the initial training phase, coefficients align contingent upon input–output correlation, iteratively refining alignment thereafter. Hormonal coefficients, including activation function, net function, and weight, exert influence on node components. The EANN model output, integrating the three hormones H_a, H_b, and H_c, is expressed as Eq. (22)[56]:

$$Y_i = \underbrace{\left(\gamma_i + \sum\nolimits_h \partial_{i,h} H_h\right)}_{1} \times f\left(\sum_j \left[\underbrace{\left(\beta_i + \sum\nolimits_h \chi_{i,h} H_h\right)}_{2} \times \underbrace{\left(\alpha_{i,j} + \sum\nolimits_h \Phi_{i,j,k} H_h\right) X_{i,j}}_{3} + \underbrace{\left(\alpha_i + \sum\nolimits_h \chi_{i,h} H_h\right)}_{4}\right]\right) \tag{22}$$

where h, i, and j represent input neurons, hidden, and output layers, respectively, and f denotes an activation function [57–59]. Figure 1 shows the framework of the study plan using machine-learning, numerical and experimental models.

The choice of EANN for this study is based on several key advantages that it offers over traditional machine learning models. EANNs are particularly well-suited for handling datasets with limited data points, which is often a constraint in solar panel performance studies due to the variability in environmental conditions and the cost of extensive data collection. EANNs incorporate emotional factors into the learning process, which enhances their ability to predict peak values accurately[59,60]. This capability is crucial for optimizing the maximum power point (MPP) of solar panels, ensuring efficient energy conversion under fluctuating conditions. Traditional neural networks and other machine learning models like support vector machines (SVM) and ANN require large datasets to achieve high accuracy. However, EANNs can effectively learn from smaller datasets by simulating human emotional responses, thus improving their generalization ability. Additionally, EANNs have been shown to outperform conventional models in predicting non-linear and complex patterns, which are inherent in the environmental conditions affecting solar panel performance.

The data collection process for this study involved the systematic measurement of both operational and environmental parameters of the solar panel system. Measurements were taken over a continuous period from 7:00 to 17:00 to capture a full day's variation in environmental conditions. The key environmental parameters recorded included solar radiation, wind speed, and ambient temperature. These parameters were measured using high-precision sensors calibrated to ensure accuracy and reliability. Data was collected at 15-min intervals to ensure a detailed and granular dataset that captures the dynamic changes in environmental conditions throughout the day. The measurements were conducted over a span of 3 days to account in constant weather conditions, thus providing a robust dataset for model training and validation. The operational parameters of the solar panel system, such as open-circuit voltage, short-circuit current, system resistances, and maximum power point characteristics, were also recorded. All collected data were logged into a central database for preprocessing. The preprocessing steps included data cleaning to remove any anomalies or outliers, normalization (based on Eq. 22) to ensure consistency, and integration of environmental and operational datasets. This prepared data set was then used for training the EANN model.

$$X = \frac{T_i - T_{min}}{T_{max} - T_{min}} \tag{23}$$

where, X is normalized value, T_i is real value of data before normalization, and T_{min} and T_{max} pre-normalization minimum and maximum value, respectively [61].

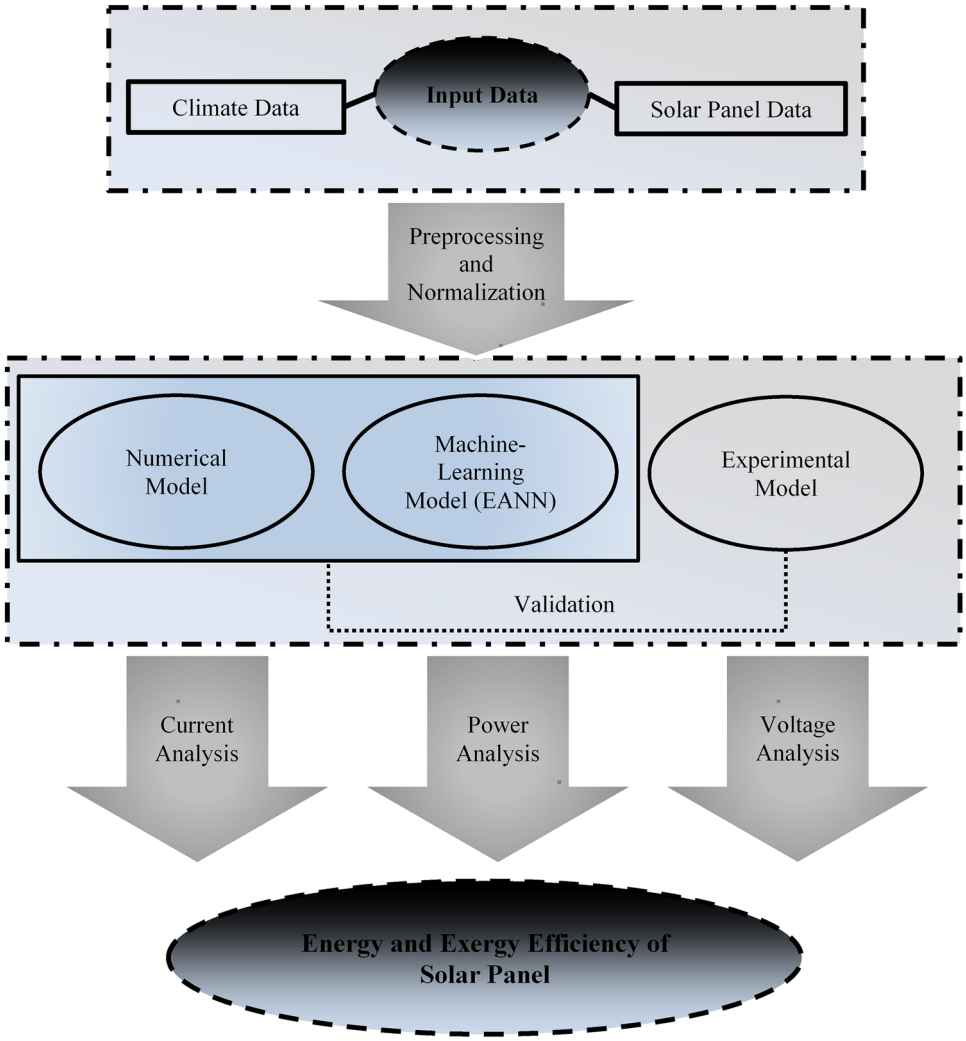

Fig. 1. The framework of the study based on proposed model.

Input data specification

The choice of specific input parameters for the emotional artificial neural network (EANN) model was based on their significant influence on the performance and efficiency of solar panels. The selected parameters include environmental factors such as solar radiation, wind speed, and ambient temperature, as well as operational parameters such as open-circuit voltage (Voc), short-circuit current (Isc), system resistances, and maximum power point (MPP) characteristics.

Solar radiation is the primary energy source for photovoltaic systems, directly affecting the amount of electrical energy generated by the solar panel. Variations in solar radiation intensity significantly influence the panel's output. Accurate measurement and inclusion of solar radiation data enhance the model's ability to predict energy output, as it directly correlates with the solar panel's performance under different lighting conditions. Wind speed affects the cooling of the solar panel, which in turn influences its efficiency. Higher wind speeds can reduce the panel's temperature, mitigating efficiency losses due to overheating. Including wind speed as an input parameter improves the model's reliability in predicting performance under varying environmental conditions, especially in regions with significant wind activity. Ambient temperature affects the thermal characteristics of the solar panel. Higher temperatures can decrease the panel's efficiency, while lower temperatures can enhance it. By accounting for ambient temperature, the model can more accurately predict the panel's efficiency and output across different temperature ranges, improving overall prediction accuracy.

Voc is a critical indicator of the potential maximum voltage output of the solar panel when no load is applied. It reflects the panel's capability to generate voltage under optimal conditions. Including Voc in the model helps in predicting the voltage behavior of the solar panel, contributing to more accurate simulations of its performance under varying load conditions. Isc represents the maximum current output when the solar panel's terminals are shorted. It is a fundamental parameter for assessing the panel's current-generating capacity. The inclusion of Isc enhances the model's ability to predict the current output under different operational states, thereby increasing the reliability of the performance predictions. The resistances within the solar panel system, including series and shunt resistances, affect the flow of current and overall efficiency. High resistances can lead to power losses.

By considering system resistances, the model can more accurately simulate the internal electrical behavior of the solar panel, leading to better predictions of efficiency and power output. MPP characteristics determine the voltage and current at which the solar panel produces its maximum power. This is crucial for optimizing energy extraction. Including MPP characteristics in the model ensures that it can accurately predict the conditions under which the panel operates most efficiently, thereby enhancing the model's reliability in practical applications.

Sensitivity analysis was performed to determine how variations in each input parameter affect the model's output. A one-at-a-time (OAT) approach was used, where each input parameter was varied within its realistic operational range while keeping the other parameters constant. The percentage change in the model's output (energy efficiency, power output) was recorded to quantify the sensitivity. The analysis revealed that solar radiation and MPP characteristics are the most sensitive parameters, significantly influencing energy output and efficiency. Ambient temperature and wind speed showed moderate sensitivity, affecting thermal and cooling dynamics, respectively. Voc, Isc, and system resistances also demonstrated notable sensitivity, impacting the electrical behavior and efficiency of the solar panel (Table 3).

Results and discussion

Figure 2 displays the current and power diagram in relation to voltage under the parameters of a radiation intensity of 1000 watts per square meter and a temperature of 24 °C. This information is then compared to the specifications provided by the panel manufacturer. The validity of solar energy has been confirmed.

The power and current shows that were derived from the modeling and those that were provided by the manufacturer are shown to have a tight relationship in Fig. 2. It is clear that there is a high degree of accuracy given the significant degree of overlap. The process of developing a model is what it is called. When it comes to evaluating the accuracy of the results, the root mean square error is a suitable statistic to use. This quantity allows for the investigation of the impact of increasing errors in the measured data on the accuracy of the estimation. Equation (23) determines the magnitude of this error.

$$e_{rms} = \sqrt{\frac{1}{n}\sum_{i=1}^{n}\left(I_{Num} - I_{Exp}\right)^2}, e_{rms} = \sqrt{\frac{1}{n}\sum_{i=1}^{n}\left(P_{\mathrm{Num}} - P_{Exp}\right)^2} \tag{23}$$

The current and power diagrams are depicted in Figs. 3 and 4, respectively, with respect to voltage at a temperature of 25 °C and in accordance with the varying intensities of different radiations.

Figure 3 illustrates that there is a direct connection between the increase in radiation intensity and the growth in the short-circuit current. When the strength of radiation is increased, the increase in voltage displays a logarithmic relationship with the intensity of the radiation. The current in the short circuit is exactly proportional to the radiation level and remains essentially constant regardless of the voltage. This relationship continues until the short circuit current approaches the voltage in the open circuit. If we assume that the radiation that strikes the

Input data	Impact on model output (%)
Solar radiation	13
Ambient temperature	7
Wind speed	4
Open-circuit voltage (Voc)	10
Short-circuit current (Isc)	11
System resistances	5
MPP characteristics	9

Table 3. Sensitivity analysis results.

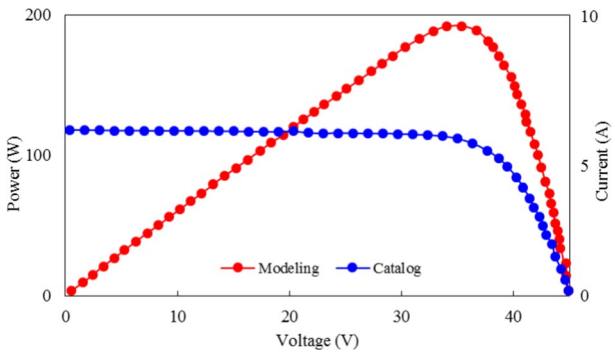

Fig. 2. A comparison between numerical model results and solar panel specification data.

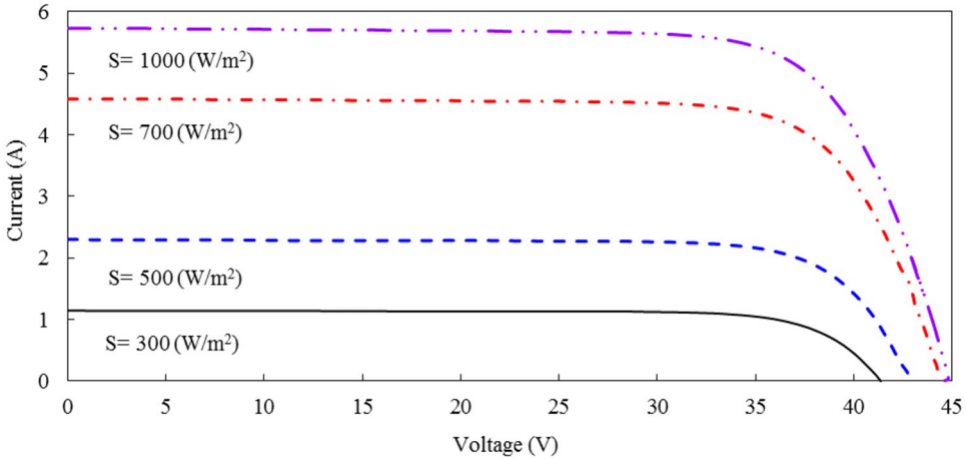

Fig. 3. System current variation by voltage in deferent solar radiation intensity level.

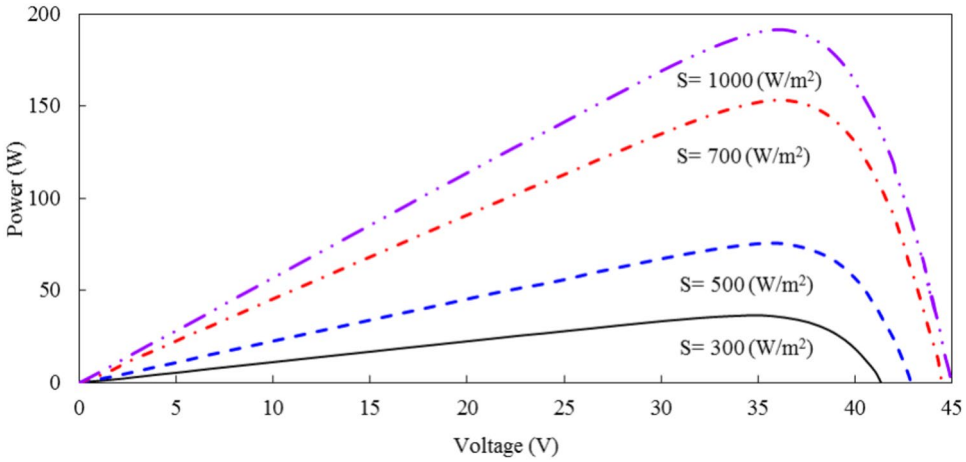

Fig. 4. System power output based on voltage across various radiation intensity level.

surface has a consistent emission spectrum, then we can consider the short circuit current to be a trustworthy indicator of the quantity of radiation that is incident on the surface, and vice versa. This is made possible by the assumption that the temperature remains constant. As the intensity of the radiation increases while maintaining the same temperature, the amount of energy that is introduced into the system also increases.

Therefore, as depicted in Fig. 4, the output power is seeing an upward trend. Applying a specific voltage results in a proportional increase in power, which is equivalent to an increase in the magnitude of electric current. It is important to note that the current is not influenced by any other elements. The relationship between voltage and power exhibits a nearly linear correlation when the voltage is not significantly elevated. Figures 3 and 4 not only validate the fundamental physics of the models but also give mutually supportive data.

As depicted in Figs. 3 and 4, there is a clear increase in short-circuit current (Isc) with rising radiation intensity. This relationship is approximately linear, confirming that the short-circuit current is directly proportional to the incident radiation intensity. This implies that at higher radiation levels, more photons are available to generate electron–hole pairs, thereby increasing the current. The voltage, however, exhibits a logarithmic increase with radiation intensity, indicating that while more carriers are generated, the voltage increases at a diminishing rate due to recombination effects and the intrinsic properties of the photovoltaic material.

Furthermore, as the voltage disparity escalates and nears the open circuit voltage, the current experiences a quick decline, as anticipated. Consequently, the power diminishes until both values hit zero at the open circuit voltage. The current and power diagrams are depicted in Figs. 5 and 6, respectively, using voltage as the variable. These diagrams are based on a constant radiation intensity of 1000 watts per square meter and varying temperatures.

Figure 5 demonstrates that when temperature rises, the open circuit voltage experiences a significant fall, whereas the short circuit current shows a little increase. The fall in temperature causes a reduction in the energy gap of semiconductors, which, as Eq. (10), leads to a logarithmic dependency of the current I_o on the energy gap. Consequently, the voltage reduces rapidly. It is evident that increasing temperature leads to a significant

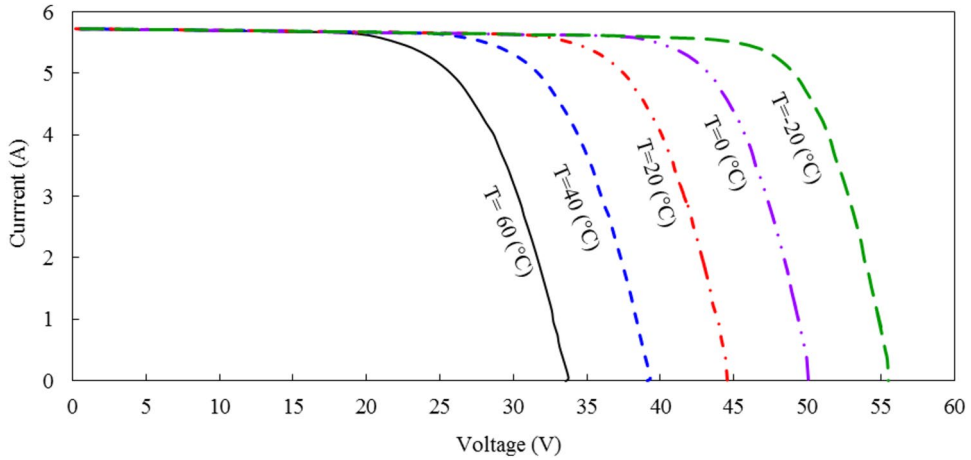

Fig. 5. Temperature effect on system current output in deferent voltage.

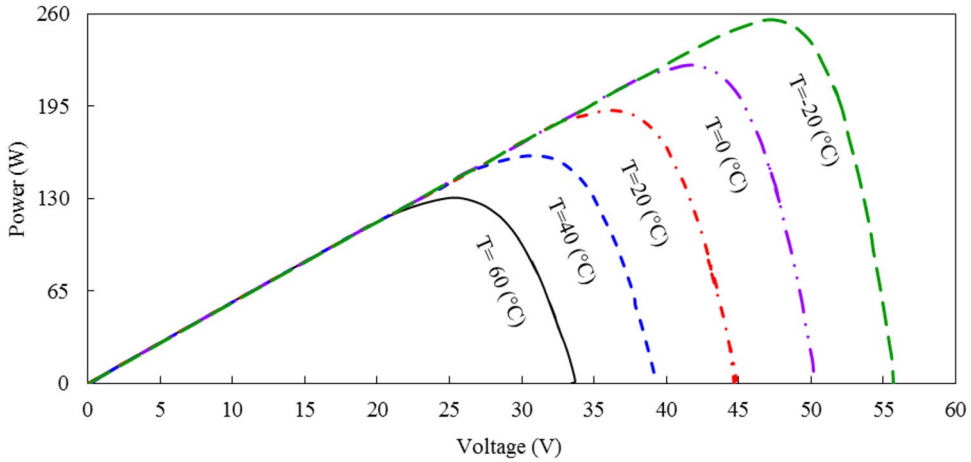

Fig. 6. Temperature effect on system power output in deferent voltage.

reduction in open-circuit voltage (Voc), whereas the short-circuit current (Isc) experiences a slight increase. This is attributed to the temperature-induced reduction in the semiconductor bandgap, which decreases Voc. The minor increase in Isc with temperature can be linked to enhanced carrier generation. The overall effect is a reduction in the power output at higher temperatures, underscoring the importance of effective thermal management in photovoltaic systems.

As illustrated in Fig. 6, there is a marked decline in open-circuit voltage, which in turn results in a proportional decrease in maximum power, particularly noticeable at lower voltage levels. This phenomenon is more frequently observed at these lower voltage levels and can be attributed to the intrinsic correlation between voltage, current in an open circuit, and the energy gap of semiconductors. Additionally, much like Fig. 4, this graph demonstrates that a specific voltage threshold must be attained to achieve maximum power output, irrespective of temperature. Upon increasing the temperature to 100 °C, there is a significant reduction in voltage of approximately 40%. Furthermore, the figure indicates a direct relationship between the voltages corresponding to the maximum power point and the maximum power output at various temperatures.

Figure 7 depicts the variations in ambient temperature, wind speed, and cell temperature that the two approaches mentioned in Eq. (19) predicted would occur over the course of the test period. Based on these diagrams, the wind speed fluctuates by 6 m per second. The second technique is more precise than the first because it takes into account the impact of wind speed, energy efficiency, and panel radiation characteristics on the cell's temperature. This method serves as the foundation for the calculations. The data indicates that wind speed plays a critical role in moderating cell temperature, which in turn affects the efficiency of photovoltaic cells. The detailed analysis of these figures underscores the significant impact of temperature and solar radiation intensity on the performance parameters of PV cells. The precise method incorporating wind speed and radiation characteristics offers a more accurate prediction of cell temperature and performance, reinforcing the necessity of comprehensive environmental considerations in photovoltaic system design and analysis.

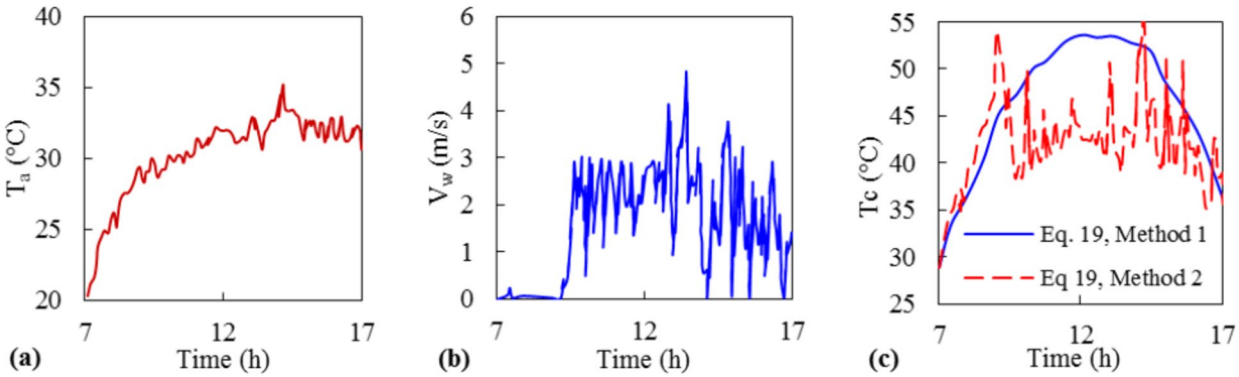

Fig. 7. Environmental ccondition variations (**a**) ambient temperature, (**b**) wind speed and (**c**) cell temperature, during the day.

Figure 8 presents the solar radiation intensity measured throughout the day, comparing experimental data, numerical model predictions, and the proposed model's predictions. The figure reveals several key insights into the variability in solar radiation and its impact on the efficiency of solar panels.

The variability in efficiency rates can be attributed to several factors, notably the fluctuations in solar radiation intensity. As indicated in Fig. 8, the solar radiation intensity exhibits significant variation from early morning (around 7:00 AM) to late afternoon (around 5:00 PM). The experimental data show a sharp increase in radiation intensity starting from approximately 7:00 AM, reaching its peak between 12:00 PM and 1:00 PM, and then gradually declining towards the evening.

This diurnal pattern of solar radiation is crucial for understanding the efficiency of solar panels. During peak radiation hours, the efficiency of solar panels is generally higher due to the increased availability of solar energy. However, the efficiency is not constant and tends to fluctuate due to transient environmental factors such as cloud cover, atmospheric conditions, and potential shading. The experimental data exhibit more fluctuations compared to the numerical and proposed models. This suggests the influence of transient atmospheric conditions such as cloud cover, which can cause rapid changes in radiation intensity. These short-term variations are often not fully captured by numerical models, which tend to smooth out such fluctuations.

As the temperature rises throughout the day, it can negatively impact the efficiency of solar panels. Elevated temperatures can increase the internal resistance of the photovoltaic cells, leading to reduced voltage output and overall efficiency. This thermal effect, combined with the varying intensity of solar radiation, creates a complex dynamic affecting the solar panel's performance. Wind speed can also play a role in modulating the temperature of the solar panels. Higher wind speeds can enhance convective cooling, thereby reducing the temperature of the panels and potentially improving their efficiency. The proposed model, which takes into account wind speed and other environmental factors, shows a closer alignment with the experimental data than the purely numerical model. When compared with similar studies, the observed variability in efficiency rates aligns with findings reported in the literature. For instance, studies by Dajuma et al.[62] and Wang et al.[63] have demonstrated that solar panel efficiency is highly sensitive to both solar radiation intensity and environmental conditions. These studies corroborate the significant impact of transient factors such as cloud cover and temperature on the performance of solar panels.

To determine the output power, it is essential to calculate the voltage and current at the moment of highest power throughout the day, using Eq. (13). Figures 9, 10 and 11 display the current and voltage diagram at the point of highest power, as well as the variations in maximum power during the day.

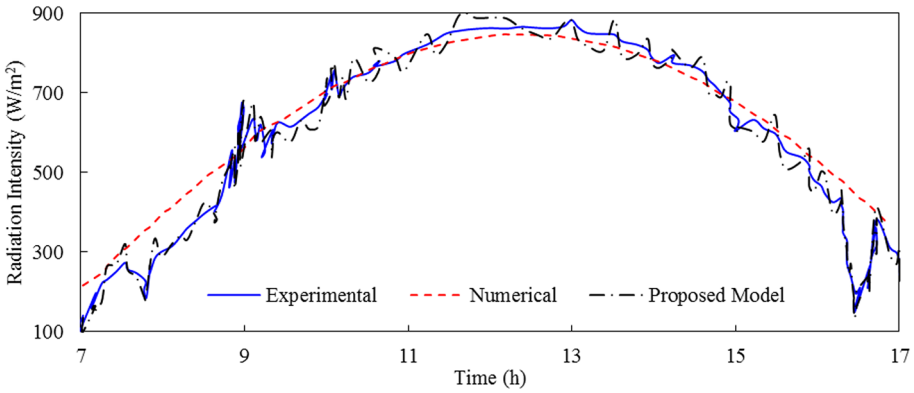

Fig. 8. The results of solar radiation intensity during the day using different models.

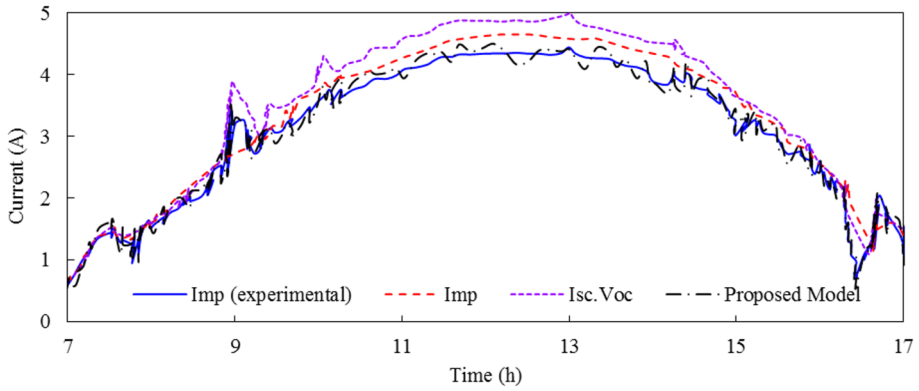

Fig. 9. Current variation at the point of maximum power and short circuit current during the day.

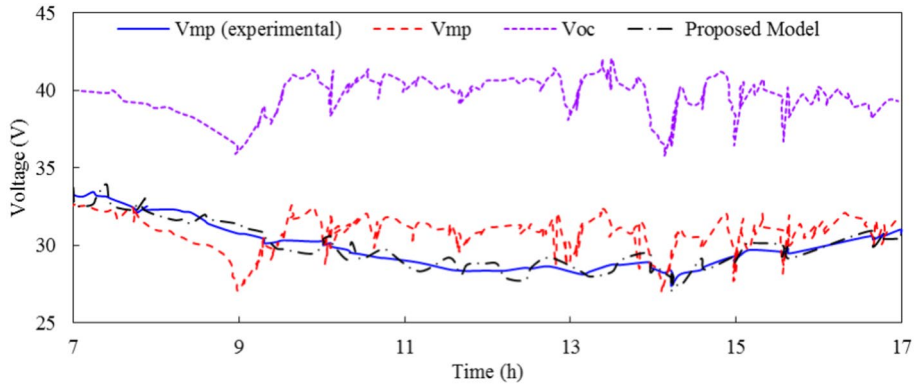

Fig. 10. Voltage variation at the point of maximum power and open circuit voltage during the day.

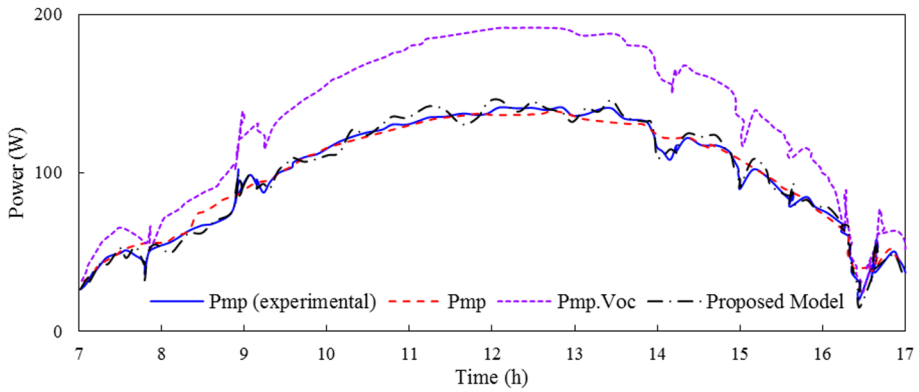

Fig. 11. Variation of maximum power during the day.

Figure 9 illustrates the current variation at the point of maximum power (Imp) and the short circuit current (Isc) throughout the day, comparing experimental data, numerical model predictions, short circuit current, and the proposed model's predictions. The experimental data for Imp shows a gradual increase in the morning, peaking around midday, and then declining in the afternoon. This trend is consistent with the daily solar radiation pattern. The numerical and proposed models closely follow the experimental data, although the proposed model shows a slightly better fit, capturing transient fluctuations more accurately. The Isc follows a similar diurnal pattern but consistently exhibits higher values than Imp. This is expected as Isc represents the maximum current generated by the solar panel under short circuit conditions, unaffected by load resistance. The current output is directly proportional to the solar radiation intensity. Peaks in current correspond to periods of high radiation, as shown in Fig. 8. Higher temperatures can reduce current output due to increased resistance within the solar cells. This thermal effect is evident in the slight midday dip observed in the experimental data for both Imp

and Isc. Kumar et al. [64] have reported similar diurnal variations in current output, affirming the impact of solar radiation and temperature on solar panel performance.

Figure 10 presents the voltage variation at the point of maximum power (Vmp) and the open circuit voltage (Voc) throughout the day, comparing experimental data, numerical model predictions, open circuit voltage, and the proposed model's predictions. The Vmp shows a relatively stable pattern with minor fluctuations throughout the day. The numerical and proposed models follow the experimental data closely, with the proposed model providing a slightly better fit. The Voc (purple dashed line) remains relatively stable, with minor fluctuations. The stability of Voc compared to Vmp is indicative of the solar panel's inherent characteristics. Voltage output is inversely proportional to temperature. Higher temperatures typically result in lower voltage outputs, which can be observed in the slight midday dip in Vmp. While radiation primarily influences current, it indirectly affects voltage through temperature changes. The voltage trends observed are consistent with findings from studies such as Nadeem et al.[65], which also report stable Voc values and minor fluctuations in Vmp due to temperature variations.

Figure 11 displays the variation in maximum power output (Pmp) throughout the day, comparing experimental data (blue solid line), numerical model predictions, maximum power point voltage (Pmp.Voc), and the proposed model's predictions. The Pmp follows a diurnal pattern, increasing in the morning, peaking around midday, and decreasing in the afternoon. The experimental data shows this trend clearly, with the proposed model providing the best fit, capturing transient fluctuations more accurately than the numerical model. The power output is a product of current and voltage, both of which are influenced by solar radiation and temperature. The observed power variation is a direct consequence of the variations in these two parameters.

Energy and exergy analysis is conducted by utilizing the outcomes of electrical modelling and experimental data. Exergy analysis is often regarded as a more suitable approach since it distinguishes between energy that can be effectively utilized and energy that cannot. Consequently, our research has prioritized the examination of exergy analysis. Figure 12 displays the quantities of input, wasted, thermal, and electrical exergy. The analysis reveals that the highest input exergy coincides with peak solar radiation around midday. However, a significant portion of this exergy is lost due to irreversibilities, primarily as thermal exergy. The electrical exergy, though relatively small, indicates the actual useful energy harnessed by the photovoltaic system. The figure underscores that despite the high input exergy, substantial improvements are necessary to reduce exergy losses and enhance overall system efficiency.

As noon approaches, the radiation intensity reaches its peak, whereas it drops as evening approaches. Generally, the input exergy may be assumed to follow the same trend, as Eq. (16) indicates that radiation intensity directly influences the input exergy. Furthermore, by comparing Figs. 8 and 12, it is evident that during midday, the most significant disparity lies between the input exergy and the radiation intensity. This implies that the variations in radiation intensity happen at a faster rate than the changes in input exergy. In simpler terms, the graph representing exergy with respect to time generally has a lower slope compared to the graph representing radiation intensity. The cause of this phenomenon is the inverse correlation between exergy and radiation, as stated in Eq. (16). This correlation hinders the increase of input exergy at elevated temperatures. While its impact is not as potent as radiation's intensity, typically the exergy tends to increase as it approaches noon, which is the time of maximum radiation intensity. However, the rise in radiation intensity also raises the temperature of the surroundings. This increase in temperature hinders the rapid growth of incoming exergy around noon. However, during the morning and evening, the fluctuations in radiation intensity align more closely with the fluctuations in input exergy. Figure 12 illustrates that around 80% of the input exergy is lost as a result of irreversibility. In the most favourable scenario, with regards to radiation intensity, only around 150 W of the input exergy is transformed into electrical exergy. The peak thermal exergy output during the day is 35 watts, indicating that solar panels, despite their numerous benefits, still have significant exergy waste and fall short of achieving satisfactory efficiency. Furthermore, it is evident that the thermal exergy accounts for around 20% of the electrical exergy. The utilization of both of these exergies in a system will inevitably lead to an increase in the exergy efficiency of that system. Photovoltaic systems that simultaneously generate useful electricity and heat will experience a substantial enhancement in efficiency due to this factor. Figure 13 illustrates the fluctuations in energy efficiency and exergy throughout the day.

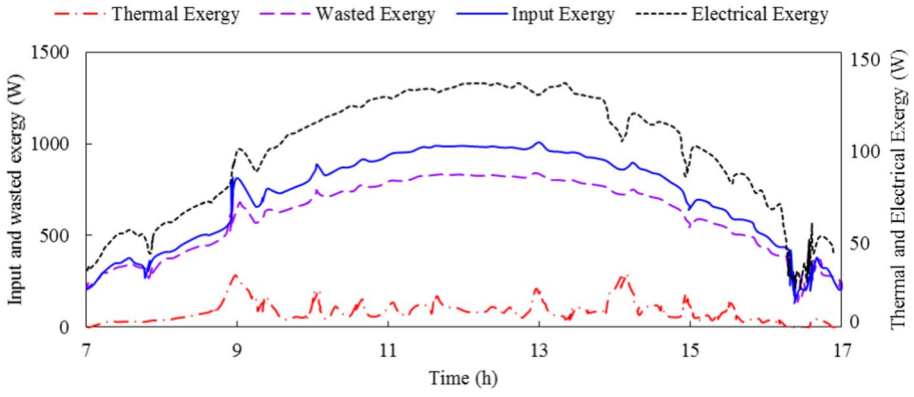

Fig. 12. System exergy analysis (Input, wasted, electrical and thermal exergy).

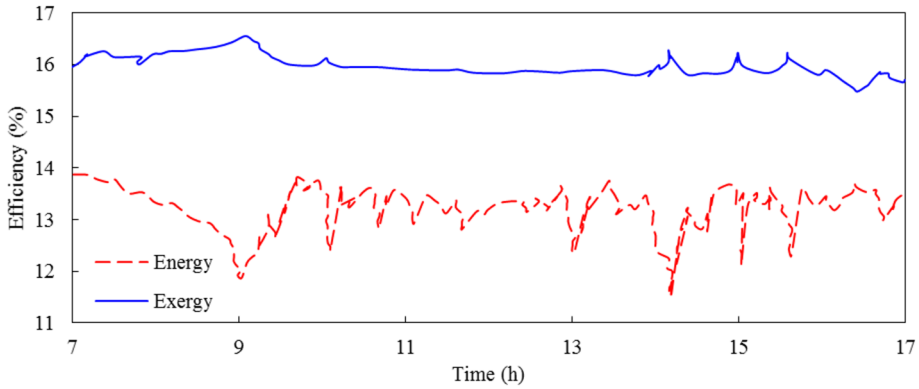

Fig. 13. System energy and exergy efficiency during the day.

Figure 13 illustrates that at approximately midday, when the input exergy reaches its maximum, there is a fall in exergy efficiency. This decline can be attributed to the rise in temperature during the peak hours of radiation, which significantly impacts the efficiency in a negative manner. This problem highlights the importance of properly addressing the cooling of the panels, which is a fundamental concern. The peak exergy efficiency is observed during the pre-noon hours, characterized by strong radiation intensity and a comparatively low temperature. The exergy efficiency reaches its minimum value at approximately 16:00, coinciding with the lowest level of radiation intensity throughout the day. Furthermore, in this particular configuration, a comparison has been made between energy efficiency and exergy. Exergy energy exhibits increased efficiency due to its ability to utilize energy that is typically considered wasted, such as heat, which is not classified as wasted exergy energy. Based on the data presented in the figure, the energy efficiency achieved during the study reaches a peak of 13%, while the exergy efficiency hits 16%. Additionally, the mean efficiency of energy and exergy for this time frame is 15% and 14%, respectively. It is worth noting that the exergy efficiency reaches its highest values at almost the same sites where it reaches its lowest values. This is because the intensity of radiation directly correlates with the increase in input exergy. The energy efficiency shows significant fluctuations throughout the day, with an overall decreasing trend from morning to afternoon. This is indicative of the solar panel's performance under varying radiation and temperature conditions. Exergy efficiency remains relatively stable throughout the day, indicating that the quality of energy conversion remains consistent despite fluctuations in environmental conditions.

Thermal energy is not included in the calculation of energy efficiency since it is not deemed beneficial. Additionally, as temperatures rise, the conversion rate of solar energy into electrical energy drops, resulting in a fall in energy efficiency. Typically, the exergy efficiency surpasses the energy efficiency in this configuration, indicating a superior ability to extract high-quality energy and consequently ensuring greater system stability. Conversely, the exergy efficiency is lower than the energy efficiency due to internal irreversible factors, indicating lower energy quality and increased system instability.

Conclusions

The objective of this study was to examine the efficiency of a 200-W solar panel by conducting thorough evaluations of its energy and exergy performance. Meteorological variables, including radiation intensity, wind speed, and temperature, were used as input data for this assessment. The accuracy of the efficiency curves was verified by comparing them with those provided by the manufacturer. A comprehensive machine-learning model utilizing an EANN was presented. Additionally, numerical and experimental models were developed to assess the efficacy of various solar cell types. The proposed model enabled the replication of electrical performance and a thorough assessment of system efficiency. Moreover, a pragmatic model was employed to validate and enhance the study by integrating experimental analysis. A complete analysis of several photovoltaic cells was provided, utilizing theoretical modeling, software creation for performance evaluation, and experimental validation. Consequently, a valuable connection between theoretical projections and practical results was established.

Initially, an analysis of thermodynamics and exergy was conducted, focusing on the principles outlined in the second law of thermodynamics and utilizing the outcomes of electrical modeling. The necessary data for analysis were obtained using experimental and in-depth methods. The solar panel's operational conditions were measured and utilized to enhance precision. The findings indicated that the average energy efficiency of the panel during daylight hours was 13.60%, with a maximum efficiency of 14.00% and a minimum efficiency of 10.34%. The panel exhibited an exergy efficiency of 15.70% on average throughout the day, with a maximum value of 16.41% and a minimum value of 13.57%. It was determined that the solar panel received an input of 1070 watts of exergy from solar radiation during peak intensity. Under optimal conditions, around 150 watts of this exergy were transformed into electrical exergy, while the remaining exergy was dissipated as thermal energy and irreversibility. The maximum thermal exergy recorded during the study period was determined to be 35 watts. Thermal exergy can be utilized for heating applications, as demonstrated in thermal photovoltaic systems.

The primary factors contributing to the enhancement of electrical power and exergy efficiency were heightened radiation intensity and reduced temperature. Consequently, the optimal operational circumstances for this solar panel were characterized by the highest radiation intensity and the lowest temperature. It was found that rising temperatures during the day had a detrimental impact on exergy efficiency and output power. Focusing

on panel cooling was identified as an effective strategy to enhance efficiency. Furthermore, the outcomes of the EANN model demonstrated that the proposed approach for predicting energy, exergy, and power was practical for simulating issues with a lower computing cost compared to the numerical model.

Future research should investigate innovative cooling methods, such as phase change materials or active cooling systems, to mitigate the adverse effects of high temperatures on photovoltaic performance. Research into new photovoltaic materials with lower temperature coefficients, such as perovskites or tandem solar cells, should be conducted to improve performance stability under varying temperatures. Dynamic models that incorporate real-time environmental data should be developed to enhance predictive accuracy and optimize energy output and efficiency in real-time, when integrated with IoT-based monitoring systems. Additionally, the integration of photovoltaic systems with other renewable energy sources, like wind or thermal energy, should be explored to provide more stable and efficient energy solutions, balancing the variability of solar power.

Practical implementations should focus on optimizing the orientation and tilt angles of photovoltaic panels based on local environmental data to maximize sunlight exposure while considering cooling effects from wind. Enhanced cooling solutions, such as heat sinks, water cooling, or air-flow enhancements, should be implemented to maintain optimal operating temperatures. Efficient energy storage systems, like advanced batteries or supercapacitors, should be integrated to store excess energy generated during peak sunlight hours and release it during lower radiation periods, ensuring a steady power supply. Policy and incentive programs that encourage the adoption of advanced photovoltaic technologies and support research into innovative materials and cooling solutions should be developed, driving industry-wide improvements in efficiency and sustainability.

This study provided useful information about the critical factors influencing photovoltaic performance. A foundation for future research and practical developments was laid. Addressing temperature management challenges and optimizing environmental conditions can significantly improve photovoltaic system efficiency and reliability, resulting in a more sustainable and energy-secure future.

This study has several limitations that should be acknowledged. One of the primary limitations is the reliance on specific meteorological data, such as radiation intensity, wind speed, and temperature, which can vary significantly depending on the geographic location and time of year. This variability may affect the generalizability of the findings to different climates and locations. Assumptions made during the study include the use of average daytime conditions for efficiency calculations, which may not account for rapid fluctuations in weather conditions that can impact solar panel performance. Additionally, the study assumes that the manufacturer-provided efficiency curves are accurate representations of the solar panel's performance under ideal conditions. Any discrepancies between these curves and real-world performance could introduce errors into the analysis. Potential sources of error include measurement inaccuracies in recording meteorological data and solar panel performance. Inherent inaccuracies in the experimental setup, such as sensor calibration errors or environmental factors not accounted for in the models, could also affect the results. The experimental validation was conducted under controlled conditions that may not fully replicate real-world scenarios, potentially limiting the applicability of the findings. Future studies should consider a broader range of environmental conditions and geographic locations to improve the generalizability of the results. Advanced modeling techniques that can dynamically adapt to changing weather conditions should be explored to provide more accurate predictions of solar panel performance. Additionally, integrating real-time monitoring and data collection systems could help reduce measurement errors and provide more reliable data for analysis.

Data availability

The datasets used and/or analysed during the current study available from the corresponding author on reasonable request.

Received: 9 April 2024; Accepted: 20 August 2024
Published online: 02 January 2025

References

1. Belge, A. T., Mishra, S. & Alegavi, S. A Review on Alternative Energy Sources. in *2022 5th International Conference on Advances in Science and Technology (ICAST)* 558–563 (IEEE, 2022). https://doi.org/10.1109/ICAST55766.2022.10039637.
2. Golenishchev-Kutuzov, A., Baysaeva, M. & Aguzarova, F. Innovation in solar energy technologies: Reducing costs and improving efficiency. In *E3S Web Conf.* **537**, 01002 (2024).
3. Shokatian-Beiragh, M., Banan-Dallalian, M., Golshani, A., Allahdadi, M. N. & Samiee-Zenoozian, M. The effectiveness of mangrove forests as a nature-based solution against flood risk under an extreme weather event. *Reg. Stud. Mar. Sci.* **77**, 103630 (2024).
4. Zhu, L. *et al.* A novel hybrid excitation magnetic lead screw and its transient sub-domain analytical model for wave energy conversion. *IEEE Trans. Energy Convers.* https://doi.org/10.1109/TEC.2024.3354512 (2024).
5. Golroudbary, S. R., Lundström, M. & Wilson, B. P. Analogical environmental cost assessment of silicon flows used in solar panels by the US and China. *Sci. Rep.* **14**, 9538 (2024).
6. Glick, A., Ali, N., Bossuyt, J., Calaf, M. & Cal, R. B. Utility-scale solar PV performance enhancements through system-level modifications. *Sci. Rep.* **10**, 10505 (2020).
7. Xinyu, W., Haoran, L. & Khan, K. Innovation in technology: A game changer for renewable energy in the European Union?. *Nat. Resour. Forum* https://doi.org/10.1111/1477-8947.12450 (2024).
8. Buonocore, J. J., Salimifard, P., Magavi, Z. & Allen, J. G. Inefficient building electrification will require massive buildout of renewable energy and seasonal energy storage. *Sci. Rep.* **12**, 11931 (2022).
9. Kuterbekov, K. A., Bekmyrza, K. Z., Kabyshev, A. M., Kubenova, M. M. & Shokatian-Beiragh, M. Fuzzy controller system utilization to increase the hydrogen production bioreactor capacity: Toward sustainability and low carbon technology. *Int. J. Low-Carbon Technol.* **19**, 667–675 (2024).
10. Molajou, A. *et al.* A new paradigm of water, food, and energy nexus. *Environ. Sci. Pollut. Res.* **30**, 107487–107497 (2021).
11. Liu, Y. *et al.* Mitigating air pollution strategies based on solar chimneys. *Sol. Energy* **218**, 11–27 (2021).
12. Xiong, H. *et al.* Numerical analysis of a negative emission technology of methane to mitigate climate change. *Sol. Energy* **255**, 416–424 (2023).

13. Fianko, S. K., Amoah, N., Jnr, S. A. & Dzogbewu, T. C. Green supply chain management and environmental performance: The moderating role of firm size. *Int. J. Ind. Eng. Manag.* **12**, 163–173 (2021).
14. Wu, Z., Yan, S., Ming, T., Zhao, X. & Zhang, N. Analysis and modeling of dust accumulation-composed spherical and cubic particles on PV module relative transmittance. *Sustain. Energy Technol. Assess.* **44**, 101015 (2021).
15. Kabeyi, M. J. B. & Olanrewaju, O. A. Sustainable energy transition for renewable and low carbon grid electricity generation and supply. *Front. Energy Res.* **9**, 743114 (2022).
16. Puspitasari, N. B., Rosyada, Z. F., Habib, F. I. & Devytasari, A. K. A. The Recommendations for implementation of green public procurement in hospitals. *Int. J. Ind. Eng. Manag.* **13**, 1–7 (2022).
17. Li, J., Lu, T., Yi, X., An, M. & Hao, R. Energy systems capacity planning under high renewable penetration considering concentrating solar power. *Sustain. Energy Technol. Assess.* **64**, 103671 (2024).
18. Inayat, S. M. *et al.* Risk assessment and mitigation strategy of large-scale solar photovoltaic systems in Pakistan. *Int. J. Ind. Eng. Manag.* **14**, 105–121 (2023).
19. Ahmadi, M. H., Ghazvini, M., Sadeghzadeh, M., Alhuyi Nazari, M. & Ghalandari, M. Utilization of hybrid nanofluids in solar energy applications: A review. *Nano-Struct. Nano-Objects* **20**, 100386 (2019).
20. Li, J. *et al.* Concentrated solar power for a reliable expansion of energy systems with high renewable penetration considering seasonal balance. *Renew. Energy* **226**, 120089 (2024).
21. Khatibi, A., Razi Astaraei, F. & Ahmadi, M. H. Generation and combination of the solar cells: A current model review. *Energy Sci. Eng.* **7**, 305–322 (2019).
22. Ashouri, M. *et al.* Exergy and exergo-economic analysis and optimization of a solar double pressure organic Rankine cycle. *Therm. Sci. Eng. Prog.* **6**, 72–86 (2018).
23. Sharma, J. *et al.* A novel long term solar photovoltaic power forecasting approach using LSTM with Nadam optimizer: A case study of India. *Energy Sci. Eng.* **10**, 2909–2929 (2022).
24. Amar, M. *et al.* Energy, exergy and economic (3E) analysis of flat-plate solar collector using novel environmental friendly nanofluid. *Sci. Rep.* **13**, 411 (2023).
25. Brenner, L., Tillenkamp, F. & Ghiaus, C. Exergy performance and optimization potential of refrigeration plants in free cooling operation. *Energy* **209**, 118464 (2020).
26. Ahamad, T., Parvez, M., Lal, S., Khan, O. & Idrisi, M. J. 4-E analysis and multiple objective optimizations of a novel solar-powered cogeneration energy system for the simultaneous production of electrical power and heating. *Sci. Rep.* **13**, 22246 (2023).
27. Ganguly, G. Improved sustainability of solar panels by improving stability of amorphous silicon solar cells. *Sci. Rep.* **13**, 10512 (2023).
28. Khalili, Z., Sheikholeslami, M. & Momayez, L. Hybrid nanofluid flow within cooling tube of photovoltaic-thermoelectric solar unit. *Sci. Rep.* **13**, 8202 (2023).
29. Rathore, N., Panwar, N. L., Yettou, F. & Gama, A. A comprehensive review of different types of solar photovoltaic cells and their applications. *Int. J. Ambient Energy* **42**, 1200–1217 (2021).
30. Hayat, M. B., Ali, D., Monyake, K. C., Alagha, L. & Ahmed, N. Solar energy-A look into power generation, challenges, and a solar-powered future. *Int. J. Energy Res.* **43**, 1049–1067 (2019).
31. Rahman, A., Farrok, O. & Haque, M. M. Environmental impact of renewable energy source based electrical power plants: Solar, wind, hydroelectric, biomass, geothermal, tidal, ocean, and osmotic. *Renew. Sustain. Energy Rev.* **161**, 112279 (2022).
32. Alfalari, A. & Alaiwi, Y. Investigation of the effective factors on solar powered fixed-wing UAV for extended flight endurance. In *2022 International Symposium on Multidisciplinary Studies and Innovative Technologies (ISMSIT)* 828–833 (IEEE, 2022). https://doi.org/10.1109/ISMSIT56059.2022.9932721.
33. Alaiwi, Y., Taha, A. & ALjumaili, Y. Enhancement of the polycrystalline solar panel performance using a heatsink cooling system with PCM. *Int. J. Eng. Artif. Intell.* **4**, 24–34 (2023).
34. Nguyen, H. Q. & Shabani, B. Proton exchange membrane fuel cells heat recovery opportunities for combined heating/cooling and power applications. *Energy Convers. Manag.* **204**, 112328 (2020).
35. Krishan, O. & Suhag, S. An updated review of energy storage systems: Classification and applications in distributed generation power systems incorporating renewable energy resources. *Int. J. Energy Res.* **43**, 6171–6210 (2019).
36. Allouhi, A., Benzakour Amine, M., Buker, M. S., Kousksou, T. & Jamil, A. Forced-circulation solar water heating system using heat pipe-flat plate collectors: Energy and exergy analysis. *Energy* **180**, 429–443 (2019).
37. Mohammed, M. K., Al Doori, W. H., Jassim, A. H., Ibrahim, T. K. & Al-Sammarraie, A. T. Energy and exergy analysis of the steam power plant based on effect the numbers of feed water heater. *J. Adv. Res. Fluid Mech. Therm. Sci.* **56**, 211–222 (2019).
38. Makhdoomi, S. & Askarzadeh, A. Impact of solar tracker and energy storage system on sizing of hybrid energy systems: A comparison between diesel/PV/PHS and diesel/PV/FC. *Energy* **231**, 120920 (2021).
39. Hatami, S., Payganeh, G. & Mehrpanahi, A. Energy and exergy analysis of an indirect solar dryer based on a dynamic model. *J. Clean. Prod.* **244**, 118809 (2020).
40. Ghadikolaei, S. S. C. Solar photovoltaic cells performance improvement by cooling technology: An overall review. *Int. J. Hydrog. Energy* **46**, 10939–10972 (2021).
41. Sharaf, M., Yousef, M. S. & Huzayyin, A. S. Review of cooling techniques used to enhance the efficiency of photovoltaic power systems. *Environ. Sci. Pollut. Res.* **29**, 26131–26159 (2022).
42. Ali Sadat, S., Faraji, J., Nazififard, M. & Ketabi, A. The experimental analysis of dust deposition effect on solar photovoltaic panels in Iran's desert environment. *Sustain. Energy Technol. Assess.* **47**, 101542 (2021).
43. Jaszczur, M., Koshti, A., Nawrot, W. & Sędor, P. An investigation of the dust accumulation on photovoltaic panels. *Environ. Sci. Pollut. Res.* **27**, 2001–2014 (2020).
44. AlShafeey, M. & Csáki, C. Evaluating neural network and linear regression photovoltaic power forecasting models based on different input methods. *Energy Rep.* https://doi.org/10.1016/j.egyr.2021.10.125 (2021).
45. Nwokolo, S. C., Obiwulu, A. U., Ogbulezie, J. C. & Amadi, S. O. Hybridization of statistical machine learning and numerical models for improving beam, diffuse and global solar radiation prediction. *Clean. Eng. Technol.* **9**, 100529 (2022).
46. Faria, V. A. D., Bernardes, J. V. & Bortoni, E. C. Parameter estimation of synchronous machines considering field voltage variation during the sudden short-circuit test. *Int. J. Electr. Power Energy Syst.* **114**, 105421 (2020).
47. Kirtley, J. L. *Electric power principles: Sources, conversion, distribution and use* 2nd edn. (Wiley, 2019). https://doi.org/10.1002/9781119585305.
48. Farahmand, M. Z., Nazari, M. E., Shamlou, S. & Shafie-khah, M. The simultaneous impacts of seasonal weather and solar conditions on PV panels electrical characteristics. *Energies* **14**, 845 (2021).
49. Hasan, A. & Dincer, I. A new performance assessment methodology of bifacial photovoltaic solar panels for offshore applications. *Energy Convers. Manag.* **220**, 112972 (2020).
50. Hajatzadeh Pordanjani, A., Aghakhani, S., Karimipour, A., Afrand, M. & Goodarzi, M. Investigation of free convection heat transfer and entropy generation of nanofluid flow inside a cavity affected by magnetic field and thermal radiation. *J. Therm. Anal. Calorim.* **137**, 997–1019 (2019).
51. Alnaqi, A. A. *et al.* Effects of magnetic field on the convective heat transfer rate and entropy generation of a nanofluid in an inclined square cavity equipped with a conductor fin: Considering the radiation effect. *Int. J. Heat Mass Transf.* **133**, 256–267 (2019).

52. Wang, H., Han, D., Cui, M. & Chen, C. NAS-YOLOX: A SAR ship detection using neural architecture search and multi-scale attention. *Connect. Sci.* **35**, 1–32 (2023).
53. Xie, G. *et al.* A gradient-enhanced physics-informed neural networks method for the wave equation. *Eng. Anal. Bound. Elem.* **166**, 105802 (2024).
54. Nourani, V. An emotional ANN (EANN) approach to modeling rainfall-runoff process. *J. Hydrol.* **544**, 267–277 (2017).
55. Molajou, A., Nourani, V., Afshar, A., Khosravi, M. & Brysiewicz, A. Optimal design and feature selection by genetic algorithm for emotional artificial neural network (EANN) in rainfall-runoff modeling. *Water Resour. Manag.* **35**, 2369–2384 (2021).
56. Beirami, A. A. M. *et al.* An assessment of greenhouse gases emission from diesel engine by adding carbon nanotube to biodiesel fuel using machine learning technique. *Int. J. Low-Carbon Technol.* **19**, 1358–1367 (2024).
57. Sharghi, E., Nourani, V., Najafi, H. & Molajou, A. Emotional ANN (EANN) and Wavelet-ANN (WANN) approaches for Markovian and seasonal based modeling of rainfall-runoff process. *Water Resour. Manag.* **32**, 3441–3456 (2018).
58. Haruna, S. I. *et al.* Compressive strength of self-compacting concrete modified with rice husk ash and calcium carbide waste modeling: A feasibility of emerging emotional intelligent model (EANN) versus traditional FFNN. *Arab. J. Sci. Eng.* **46**, 11207–11222 (2021).
59. Sharghi, E., Nourani, V., Molajou, A. & Najafi, H. Conjunction of emotional ANN (EANN) and wavelet transform for rainfall-runoff modeling. *J. Hydroinform.* **21**, 136–152 (2019).
60. Nourani, V., Molajou, A., Najafi, H. & Danandeh Mehr, A. Emotional ANN (EANN): A new generation of neural networks for hydrological modeling in IoT. In *Artificial intelligence in IoT transactions on computational science and computational intelligence* (ed. Al-Turjman, F.) 45–61 (Springer, 2019). https://doi.org/10.1007/978-3-030-04110-6_3.
61. Chen, T. C. *et al.* Evaluation of hybrid soft computing model's performance in estimating wave height. *Adv. Civ. Eng.* **2023**, 1–13 (2023).
62. Dajuma, A. *et al.* Sensitivity of solar photovoltaic panel efficiency to weather and dust over West Africa: Comparative experimental study between Niamey (Niger) and Abidjan (Côte d'Ivoire). *Comput. Water Energy Environ. Eng.* **5**, 123–147 (2016).
63. Wang, Z., Li, Y., Wang, K. & Huang, Z. Environment-adjusted operational performance evaluation of solar photovoltaic power plants: A three stage efficiency analysis. *Renew. Sustain. Energy Rev.* **76**, 1153–1162 (2017).
64. Kumar, M. S., Balasubramanian, K. R. & Maheswari, L. Effect of temperature on solar photovoltaic panel efficiency. *Int. J. Eng. Adv. Technol.* **8**, 2593–2595 (2019).
65. Nadeem, A., Sher, H. A., Murtaza, A. F. & Ahmed, N. An online fractional open-circuit voltage maximum power point tracking (MPPT) algorithm based on sliding mode control. In *2020 International Symposium on Recent Advances in Electrical Engineering & Computer Sciences (RAEE & CS)* 1–6 (IEEE, 2020). https://doi.org/10.1109/RAEECS50817.2020.9265809.

Acknowledgements

The authors extend their appreciation to the Deanship of Scientific Research at King Khalid University under for funding this work through General Research Project under Grant number (RGP.2/33/45).

Author contributions

A.B.: Methodology, software, data curation, validation, resources. S.O.: Methodology, software, data curation, validation, formal analyses. Z.M.S.E.: Conceptualization, methodology, validation, investigation, formal analyses. F.A.: Data curation, software, writing-reviewing and editing, investigation, resources. N.E.B.: Software, writing-reviewing and editing, investigation.

Competing interests

The authors declare no competing interests.

Additional information

Correspondence and requests for materials should be addressed to Z.M.S.E. or N.E.B.